Computational fluid dynamics–based modeling and optimization of flow rate and radiant exitance for 1,4-dioxane degradation in a vacuum ultraviolet photoreactor

Gang Shi[a], Shota Nishizawa[a], Taku Matsushita[b,*], Yuna Kato[a], Takahiro Kozumi[a], Yoshihiko Matsui[b], and Nobutaka Shirasaki[b]

[a]Graduate School of Engineering, Hokkaido University, N13W8, Sapporo, 060-8628, Japan
[b]Faculty of Engineering, Hokkaido University, N13W8, Sapporo, 060-8628, Japan

*Corresponding author. E-mail address: taku-m@eng.hokudai.ac.jp (T. Matsushita)

Abstract: 1,4-Dioxane is one of the most persistent organic micropollutants in conventional drinking-water-treatment processes. Vacuum ultraviolet (VUV) treatment is a promising means of removing micropollutants such as 1,4-dioxane from source water, but this approach has not yet been implemented in a full-scale water treatment plant, partly because the operating parameters for pilot and full-scale VUV photoreactors have not been optimized. Here, we developed a computational fluid dynamics–based method for optimizing VUV photoreactor performance through energy-based analyses that take into account the effects of two important operating parameters—flow rate and radiant exitance. First, we constructed a computational fluid dynamics model and determined the sole parameter required for the model, the pseudo-first-order rate constant for the reaction of 1,4-dioxane, by simple batch experiment. Then, we validated the model by using a pilot-scale flow-through annular photoreactor. Finally, we used the validated model to examine the effects of flow rate and radiant exitance on the efficiency of 1,4-dioxane degradation in a virtual annular photoreactor. Radiation efficiency, which was defined as the ratio of the logarithmic residual ratio of 1,4-dioxane to the theoretical minimum logarithmic residual ratio (best possible performance) under the given operating conditions, was calculated as an energy-based index of cost-effectiveness. Radiation efficiency was found to increase with increasing flow rate but decreasing radiant exitance. An electrical energy per order (EEO) analysis suggested that VUV treatment under laminar flow was most economical when low-power lamps and a high flow rate were used. In contrast, VUV treatment under turbulent flow was suggested to be most economical when high-power lamps were used at a high flow rate.

Keywords: Advanced oxidation process, Modeling, Radiation efficiency, EEO

Highlights:
1. Computational fluid dynamics model was developed to optimize photoreactor parameters
2. Model was validated for 1,4-dioxane by using a pilot-scale flow-through photoreactor
3. The model revealed that radiation efficiency increased with increasing flow rate
4. Radiation efficiency increased with decreasing radiation exitance
5. Low/high-power lamps are recommended for laminar/turbulent flow, respectively

1. Introduction

1,4-dioxane has received growing social and scientific attention due to its ubiquitous presence in the aquatic environment (Stepien et al., 2014). 1,4-Dioxane has many uses in many commercial processes (European Communities, 2004; Mohr et al., 2020), and it is found in a wide range of consumer products (e.g. detergents, shampoos, and cosmetics) as a by-product of polyester synthesis (Zenker et al., 2003). After being released into natural waters, 1,4-dioxane, which is little adsorbed by sediments ($\log K_{ow} = -0.27$; Dietz and Schnoor, 2001), eventually contaminates groundwater through recharge with contaminated surface water (Stepien et al., 2014). Toxicological studies have revealed that 1,4-

dioxane is a possible carcinogen, suggesting that using contaminated surface waters and groundwaters as sources of drinking water may increase the risk of cancer in end-users (European Communities, 2004; USEPA, 2013).

The World Health Organization suggests a guideline value of 50 μg/L for 1,4-dioxane in drinking water (WHO, 2005). However, conventional drinking-water-treatment processes (i.e. coagulation, sedimentation, activated carbon adsorption, and sand filtration) are generally ineffective at removing 1,4-dioxane from source water (McGuire et al., 1978). Ozonation and chlorination are also ineffective at degrading 1,4-dioxane (Adams et al., 1994). Indeed, some drinking-water-treatment plants in the United States were forced to close when their source waters were found to be contaminated with 1,4-dioxane (Weimar, 1980). Thus, an additional purification process is needed to improve conventional drinking-water-treatment processes.

Advanced oxidation processes involving the generation of hydroxyl radicals (OH radicals) via reaction of O_3/H_2O_2 (Suh and Mohseni, 2004), UV/TiO_2 (Coleman et al., 2007; Hill et al., 1997), or UV/H_2O_2 (Matsushita et al., 2015) are reported to degrade 1,4-dioxane. In terms of the actual application, however, these methods are constrained by the high costs of chemical storage and removal of residual chemical additives at the end of the treatment process. In contrast to these advanced oxidation processes, vacuum ultraviolet (VUV) treatment does not use chemical additives and is therefore a promising economical approach for meeting increasingly stringent drinking water standards (Imoberdorf and Mohseni, 2012; Xie et al., 2018). Indeed, in a previous laboratory-scale study, we found that VUV treatment followed by activated carbon treatment was an economical means of removing 1,4-dioxane from water without inducing the formation of by-products from coexisting natural organic matter (Matsushita et al., 2015).

However, real-world implementation of VUV treatment processes is stymied, partly because of a lack of systematic optimization of operating parameters for pilot or large-scale photoreactors (Bagheri and Mohseni, 2017). Bagheri and Mohseni (2014, 2015, 2017) have reported several computational fluid dynamics (CFD) models for analyzing the degradation of micropollutants in a VUV photoreactor. However, their models describe the effect of flow rate on micropollutant degradation under only a single flow regime (i.e. either laminar or turbulent flow), so knowledge of micropollutant degradation under different flow regimes remains limited. Moreover, their models do not consider the effect of radiant exitance, which is an important operating parameter in the VUV treatment process. For effective photoreactor operation, flow rate and radiant exitance must be optimized.

Here, we developed a CFD model that takes into consideration the effects of flow rate and radiant exitance on 1,4-dioxane degradation during VUV treatment. In our model, the chemical reaction kinetics of 1,4-dioxane were simplified to a pseudo-first-order reaction rate constant (k, m^2/J), which was determined by a simple batch degradation experiment. The model was validated via experiments carried out using a pilot-scale flow-through annular photoreactor under different flow rates and different radiant exitances. We then used the validated model to examine the effects of flow rate and radiant exitance on 1,4-dioxane degradation in a virtual annular photoreactor. Finally, the effects of flow rate and radiant exitance on treatment performance were examined by electrical energy per order (EEO) analysis. To our knowledge, this is the first study to investigate the effect of radiant exitance on photoreactor performance.

2. Materials and methods

2.1 Analytical modeling

2.1.1 Gray-box kinetic model

During VUV treatment, OH radicals form when water is irradiated by VUV photons (Imoberdorf and Mohseni, 2012; Oppenlander, 2007). Almost all of these OH radicals are generated directly from the

photolysis of water:

$$H_2O \xrightarrow{h\nu\ 185\ \text{nm}} \cdot OH + \cdot H \qquad \Phi_1 = 0.33 \tag{1}$$

$$H_2O \xrightarrow{h\nu\ 185\ \text{nm}} \cdot OH + H^+ + e^- \qquad \Phi_2 = 0.045 \tag{2}$$

where Φ_1 and Φ_2 are the quantum yields. The generated radicals react very quickly with coexisting species in the water, such as OH radical scavengers, and therefore the OH radical concentration reaches a steady-state almost immediately (De Laat et al., 1999; Sharpless and Linden, 2003). The equilibrium concentration of the OH radicals ($C_{OH,\,st}$) can be calculated using

$$C_{OH,\,st} = \frac{\Phi_1+\Phi_2}{\sum(k_i \cdot C_i)} \cdot \frac{I}{N_A E_{185}} \cdot \alpha_w \ln 10 \tag{3}$$

where k_i is the rate constant for the reaction between OH-radical-consuming species i and OH radicals, C_i is the concentration of OH-radical-consuming species i, I is the VUV fluence rate, E_{185} is the energy of a photon, N_A is Avogadro's constant, and α_w is the absorption coefficient of the pure water at 185 nm. The degradation of 1,4-dioxane occurs by reaction with OH radicals, and the other species such as Cl-related radicals have little effect on the degradation (Li et al., 2017; Matsushita et al., 2015; Patton et al., 2017); therefore, the degradation rate of 1,4-dioxane (R_d) is expressed as

$$R_d = -k_{OH} \cdot C_{OH,\,st} \cdot C \tag{4}$$

where k_{OH} is the second-order rate constant for the reaction between 1,4-dioxane and OH radicals, and C is the concentration of 1,4-dioxane. Substituting the second term in Eq. 4 with Eq. 1 gives the following expression for the rate of 1,4-dioxane degradation:

$$R_d = -k_{OH} \cdot \frac{\Phi_1 + \Phi_2}{\sum(k_i C_i)} \cdot \frac{I}{N_A E_{185}} \alpha_w \ln 10 \cdot C \tag{5}$$

The factor k_iC_i describes the reactions of all of the OH-radical-consuming species in the water. Since the number of OH-radical-consuming species is very large, the equations for the reactions of each species are not individually solved. Instead, the reactions are treated as one overall reaction with a certain rate constant (Wols et al., 2011). Accordingly, for each water, the coefficient of $-IC$ is a constant determined by the background species present in the water (water quality):

$$R_d = -k \cdot I \cdot C \tag{6}$$

where k is the apparent reaction rate constant (m^2/J). In the present study, the value of k was determined for each water via a batch degradation experiment (see Section 2.3.2).

2.1.2 CFD Lagrangian particle-tracking approach

The Lagrangian particle-tracking approach has been shown to be appropriate for the prediction of micropollutant degradation by UV treatment (Wols and Hofman-Caris, 2012a). In this approach, the term "particle" refers to a small volume of water in which VUV photon-induced reactions take place. The motion of these particles comprises an advection displacement induced by the computed velocity field, and a diffusion displacement induced by turbulent fluctuation. Both the velocity field and the diffusion are calculated by the viscous models provided by CFD software. The VUV dose (D [J/m^2]) experienced by a particle is calculated by integrating the fluence rate over the particle trajectory:

$$D = \int_0^T I(\vec{r}(t))\mathrm{d}t \tag{7}$$

where T is irradiation time, and $\vec{r}(t)$ is the position vector along the trajectory. For predicting 1,4-dioxane degradation within a particle, Eq. 6 is solved using $I(\vec{r}(t))$ of the particle trajectory from the inlet to the outlet of the reactor. The concentration at the outlet of the reactor (C) calculated using the Lagrangian approach can be simplified by using the initial concentration at the inlet (C_0) and the VUV dose (D) at the outlet:

$$C = C_0 \exp(-kD) \tag{8}$$

The concentration at the outlet ($\bar{C}$) is calculated by using the mass-flow-weighted (w_i weight of particle i, $\sum w_i = 1$) average of the concentration in each fluid particle (C_i) irradiated with the respective VUV dose (D_i) as follows:

$$\bar{C} = \sum(w_i C_i) = \sum(w_i C_0 \exp(-kD_i)) \tag{9}$$

2.1.3 Radiation efficiency

According to Jensen's inequality (Text S1), $\bar{C}$ in Eq. 9 has a minimum value $\bar{C}_{\min}$ (maximum degradation ratio) at which all the particles receive the same VUV dose $\bar{D}$ (mass-flow-weighted average VUV dose):

$$\bar{C} = \sum(w_i C_0 \exp(-kD_i)) \geq C_0 \exp\left(-k \cdot \sum w_i D_i\right)$$

$$= C_0 \exp(-k\bar{D}) = \bar{C}_{\min} \tag{10}$$

In practical terms, $\bar{D}$ can be determined as a function of VUV power input (P_{VUV}), flow rate (Q), VUV absorption coefficient (α), and water layer thickness (h) (Text S2):

$$\bar{D} = \frac{P_{\mathrm{VUV}}}{Q\alpha} \cdot (1 - 10^{-\alpha h}) \approx \frac{P_{\mathrm{VUV}}}{Q\alpha} \tag{11}$$

From a practical point of view, however, it is impossible to achieve $\bar{C}_{\min}$, because the particles do not receive a uniform VUV dose. The radiation efficiency (η) as a metric of energy-based efficiency is therefore determined as follows (Wols et al., 2015):

$$\eta \equiv \frac{\ln\left(\frac{C}{C_0}\right)}{\ln\left(\frac{\bar{C}_{\min}}{C_0}\right)} = \frac{\ln\left(\frac{C}{C_0}\right)}{-k\bar{D}} = \frac{\ln\left(\frac{C}{C_0}\right)}{-k \cdot \frac{P_{\mathrm{VUV}}}{Q\alpha}} \tag{12}$$

where $\ln(C/C_0)$ is the actual log degradation. In the present study, radiation efficiency was determined as the ratio of the actual observed degradation to the theoretical maximum achievable degradation, which assuming no variation in VUV dose among the particles.

2.2 CFD modeling

ANSYS® Workbench 2019R was used to build and discretize a 1.6-m-long pilot-scale flow-through VUV photoreactor with an annular configuration (Fig. 1). Two viscosity models in ANSYS® Fluent were used: the laminar model was used for Reynolds numbers (Re) <2000, and the realizable k-ε model coupled with standard wall function was used for Re ≥2000. The radiation field for VUV photons was computed by solving the radiative transfer equation using a non-gray discrete ordinate sub-model. The VUV inputs are summarized in Table 1. Using the Lagrangian approach, we released 4000 evenly distributed particles at the inlet. A user-defined function was used to record the VUV fluence rate along the pathline of each particle and to integrate it into the VUV dose. The concentration of 1,4-dioxane in each particle at the outlet was calculated by using Eq. 8, and the concentration of 1,4-dioxane in the whole fluid was then calculated by using Eq. 9. The computational domain of the photoreactor was divided into 2.5 million cells constituting an unstructured mesh. To guarantee proper resolution of the boundary layer, a 2-mm-layer with 10 layers of inflated prisms was placed close to the sleeve.

To investigate the effect of flow rate and radiant exitance on 1,4-dioxane degradation, a simple virtual annular photoreactor, which is a common photoreactor arrangement, was constructed by using the same model set-up procedure described above (Fig. S1). The virtual photoreactor had the same cross-section as the pilot-scale flow-through annular photoreactor, although the length was set at 1.0 m and

the whole of the photoreactor was assumed to be irradiated. Assuming fully developed laminar or turbulent flow, inlet velocity distributions at different flow rates and a given *Re* were set by using the appropriate profile in ANSYS® Fluent. Radiant exitance was defined as the direct irradiation on the external surface of the quartz sleeve. The computational domain of the photoreactor was divided into 4 million cells constituting a structured hexahedral/prism mesh.

2.3 Experimental set-up and procedures

2.3.1 Chemicals and water samples

All chemicals were purchased commercially and used without further purification. Reagent solutions for the experiments were prepared with guaranteed reagent grade chemicals and Milli-Q water (18.2 MΩ·cm, Milli-Q Advantage, Millipore Co., Bedford, MA, USA). Two types of water were used for the experiments: natural groundwater (GW) and synthetic water (SW). The GW was collected from the raw water input to a full-scale drinking-water-treatment plant (Tachikawa, Japan) and stored at 4 °C until use. No 1,4-dioxane was artificially added to the GW because it was already contaminated with 1,4-dioxane. The SW was prepared by passing laboratory tap water through an activated carbon cartridge filter (TCC-WH-T0CP, Toyo Roshi Kaisha, Japan) to remove residual free chlorine, and then adjusting the pH and alkalinity using sodium hydroxide and sodium bicarbonate, respectively, to match those of the GW. The SW was spiked with 100 μg/L of 1,4-dioxane prior to use. The main properties of the GW and SW are presented in Table S1.

2.3.2 Batch experiment for determining reaction rate constant

To determine the pseudo-first-order rate constant for the reaction of 1,4-dioxane (Eq. 6) in GW and SW, a quasi-collimated beam VUV apparatus equipped with a vacuum mercury lamp was used (Fig. 2). The distance between the top of the water to the radiation source was 30 cm. Milli-Q water spiked with 100 μg/L of 1,4-dioxane was used for comparison. The pH of the Milli-Q water was not controlled. A 100-mL glass beaker with a diameter of 4.5 cm (exposure area, 15.9 cm^2) was used as the reaction vessel. A water sample (60 mL, the path length of the quasi-collimated beam is 3.8 cm) was poured into the beaker and then covered with a wooden radiation shielding sheet until the experiment was started. Because 3.8 cm of the path length may be somewhat long compared with the depth of the layer in which the reactions between VUV photons and water molecules take place, a magnetic stirrer was used to thoroughly mix the solution during the irradiation. A 65-W low-pressure mercury lamp emitting both 185 nm (VUV) and 254 nm (UV) photons was used as the radiation source (NIQ60/35XL, Heraeus Noblelight GmbH, Hanau, Germany). To suppress the absorption of VUV photons by oxygen in the gas phase, nitrogen gas was introduced into the reactor to obtain a volume fraction of oxygen of less than 2% before turning on the lamp. To ensure a steady radiation output, the lamp was turned on at least 20 min before each experiment. A calibrated radiometer (C9536/H9535, Hamamatsu Photonics K.K., Hamamatsu, Japan) was installed parallel to the surface of the irradiated water sample to determine the fluence rate during the experiments. The VUV and UV fluence rates at the center of the vessel were 1.0 and 3.2 W/m^2, respectively. The volume-averaged VUV dose was calculated by the method described in Text S3. To observe the change in 1,4-dioxane concentration, individual experiments with an irradiation time of 3, 6, 9, or 12 min were conducted. After the irradiation, an aliquot of the solution was withdrawn, and the 1,4-dioxane remaining in the solution was quantified. The pseudo-first-order reaction rate constant in Eq. 6 was determined for the waters from the water absorption ratio ($^{\alpha_w}/_{\alpha}$) and the slope of the relationship of the natural logarithm of the residual ratio against the mean absorbed VUV dose, assuming that the irradiation was uniform because of stirring (Bolton and Stefan, 2002).

2.3.3 Pilot-scale experiment for model validation

Validation experiments were conducted using a pilot-scale flow-through VUV photoreactor made of stainless steel (Fig. 1). The internal radius of the reactor and the external radius of the quartz sleeve were 23.9 and 11.5 mm, respectively, resulting in a radial gap of 12.4 mm, which corresponded to a hydraulic diameter of 24.8 mm for the water flowing through the reactor. To provide a large range of

radiation exitance and investigate its effect in the pilot-scale photoreactor, two types of low-pressure mercury lamps (65 and 240 W, Heraeus Noblelight GmbH, Hanau, Germany) and two types of quartz sleeves with different VUV radiation transmittance were used. To mimic lower-power lamps, a 65-W lamp was coated with a synthetic fluororesin film reducing the VUV radiation exitance (Iwasaki Electric Co., Ltd., Tokyo, Japan). The lamps provided a 1.4-m-long cylindrical radiation zone within the 1.6-m photoreactor. The stable VUV and UV photon emissions on the external surface of the quartz sleeve were measured for each lamp (Table 1) by the same radiometer use in 2.3.2.

To validate the model with the respect to the effect of flow rate on 1,4-dioxane degradation, flow-through experiments were conducted with the photoreactor equipped with the 240-W lamp at room temperature using GW at flow rates ranging from 1.5 to 10.5 L/min. To validate the model with respect to the effect of radiant exitance on 1,4-dioxane degradation, similar experiments were conducted with the photoreactor equipped with different lamps and different quartz sleeves (Table 1) at room temperature using SW at a flow rate of 6.9 L/min. Samples were withdrawn from the sampling points at the inlet and the outlet, and the concentrations of 1,4-dioxane in the samples were measured.

2.3.4 Quantification methods

The concentration of 1,4-dioxane was measured by using a gas chromatograph-mass spectrometer (QP2010 Plus, Shimadzu Corporation, Kyoto, Japan) equipped with a purge and trap sample concentrator (AQUA PT 5000J Plus, GL Science Inc., Tokyo, Japan). A capillary column (HP-5MS; length 30 m, i.d. 250 μm, thickness 0.25 μm, Agilent Technologies, Palo Alto, CA, USA) was used for sample separation. The temperatures of the ion source, injector, and transfer line were controlled at 200, 180, and 180 °C, respectively. Gas chromatography-mass spectrometry was performed in the selected-ion-monitoring mode with d_8-1,4-dioxane (Fujifilm Wako Pure Chemical) as the internal standard; the fragment ions of 1,4-dioxane and d_8-1,4-dioxane were detected at m/z 88 and 96, respectively.

3. Results and discussion

3.1 Determination of reaction rate constant by batch experiment

In our model, the pseudo-first-order reaction rate constant was used to simplify the reaction of OH radicals with background OH-radical-consuming species (see Section 2.1.1). The pseudo-first-order reaction rate constant of 1,4-dioxane in each water was determined by batch experiment. In Milli-Q water (Fig. 3), 1,4-dioxane rapidly degraded to a residual ratio of approximately 5% at a volume-averaged VUV dose of 100 J/m^2. In contrast, at the similar VUV dose (100-125 J/m^2) absorbed by water, the residual ratios in SW and GW were 0.18 and 0.55, respectively, values which are much higher than that in Milli-Q water, indicating that 1,4-dioxane degradation was suppressed in SW and GW compared with in Milli-Q water. This was attributed mainly to the absorption of 185 nm radiation by chloride (Furatian and Mohseni, 2018), and scavenging of OH radicals by bicarbonate(Imoberdorf and Mohseni, 2012) and nitrate(Matsushita et al., 2019). Although the natural organic matter has been reported to scavenge OH radicals during the VUV process (Wols and Hofman-Caris, 2012b), in the present study the contribution of natural organic matter to the suppression of degradation was most likely negligible because the concentration of DOC was low, even in GW (0.09 mg/L, Table S1). The slope of the natural logarithm of the residual ratio against the mean absorbed VUV dose for SW and GW were determined to be 1.4×10^{-2} and 5.2×10^{-3} m^2/J, respectively. The reaction constants in SW and GW, calculated by these values and the water absorption ratio, were used in the CFD model simulation.

3.2 Model validation using a pilot-scale flow-through annular photoreactor

Two sets of experiments were carried out using the pilot-scale flow-through annular photoreactor: one set using different flow rates (1.5–10.5 L/min), a radiant exitance of 105 W/m^2, and GW; and one

set using different radiant exitances (7.3–105 W/m^2), a flow rate of 6.96 L/min, and SW.

Because laminar-turbulent transitional flow occurs at *Re* values between 1800 and 2800 (Darbyshire and Mullin, 2005), our use of a fully developed laminar or turbulent model may have introduced errors into the result within this *Re* range. However, the laminar model closely predicted the experimental degradation ratios obtained at *Re* values smaller than 2000, and the turbulent model closely predicted the experimental degradation ratios at *Re* values greater than 2000 (Fig. 4A). Thus, we excluded the need for any parameter fitting. Likewise, the predicted and experimental values under different radiant exitances were also similar (Fig. 4B). Overall, the model provided degradation ratios that followed the same trend as the experimental data as flow rate (*Re*) and radiant exitance were changed. Thus, we concluded that our model was valid for predicting the effects of flow rate and radiant exitance on 1,4-dioxane degradation.

In our previous research, we proposed a computational kinetic model for predicting 1,4-dioxane degradation during VUV treatment that took into account the effects of coexisting inorganic ions on the reaction kinetics (Matsushita et al., 2019); however, this model was applicable to only one operating condition (i.e. fixed flow rate and fixed radiant exitance). Although the gray-box kinetic model using the pseudo-first-order reaction rate constant in the present study may be relatively coarse compared with our previous model, we considered the present model to be able to predict 1,4-dioxane degradation with sufficient engineering accuracy under different flow rates and different radiant exitances.

3.3 Effects of flow rate on 1,4-dioxane degradation

The effects of flow rate on 1,4-dioxane degradation were examined by using our validated model and a virtual annular photoreactor (see Section 2.2). To ensure that our simulation results were reliable, the CFD Lagrangian approach used in the model was further validated. Both retention time and mass-flow-weighted average VUV dose in the virtual photoreactor calculated by our model were compared with their respective theoretical values (Fig. S2 and Text S2). Good agreement between our simulation results and the theoretical values confirmed the reliability of our model.

The effect of flow rate on 1,4-dioxane degradation was investigated by simulation with different flow rates from laminar to turbulent flow and a fixed radiant exitance of 100 W/m^2 using GW and the virtual photoreactor. The observed degradation ratios followed the same trend as that observed in the validation experiments using the pilot-scale photoreactor; that is, the degradation ratio decreased with increasing flow rate (*Re*) under the same flow regime (Fig. 5), which was attributed to the retention time of water in the reactor decreasing with increasing flow rate.

In contrast, radiation efficiency was found to increase with increasing flow rate irrespective of flow regime. The VUV radiation field in the photoreactor was non-uniform: the fluence rate decreased exponentially with distance from the lamp (Fig. S3); therefore, the VUV dose of each particle varied according to its trajectory. Under laminar flow, because water migrates in parallel layers that do not mix, the VUV fluence rate of the particle does not change along its trajectory. Thus, the VUV dose range of the particles was large (Fig. S4A) because particles close to the quartz sleeve received high VUV doses (high fluence rate and long retention time), whereas those far from the quartz sleeve received low VUV doses (low fluence rate or short retention time or both). In contrast, under turbulent flow, chaotic changes in pressure and velocity occur while the particles pass through the photoreactor, resulting in a relatively narrow dose distribution (Fig. S4B). Under both flow regimes, increasing the flow rate (*Re*) did not change the shape of the cumulative VUV dose curve, but did shift it to the left, which means that the VUV doses of all the particles decreased by the same ratio. These decreases resulted in an increase in radiation efficiency according to Jensen's inequality (Text S1).

Although our model provided values that showed the same trends as those found in the validation

experiments, discontinuous changes in degradation ratio and radiation efficiency were observed as the *Re* value was increased from 2000 to 2400. This was attributed to the use of different models for the two flow regimes (laminar model for *Re* values of ≤2000; turbulent model for *Re* values of ≥2400). The actual degradation ratio was expected to be between the values predicted by the laminar and the turbulent models in the *Re* range of 1800–2800 because the real flow in this *Re* range was laminar-turbulent transitional flow. Such transitional flow results in more physical modeling uncertainty than does fully developed laminar or turbulent flow (Versteeg and Malalasekera, 2007). To accurately predict the result for every flow rate in this range, high-resolution experiments consisting of several runs at different flow rates and a deep understanding of fluid dynamics for transitional flows would be required. However, the aim of the present study was to investigate the changes in degradation ratio and radiation efficiency for optimizing the operating parameters under fully developed laminar or turbulent flow; therefore, this discontinuity is not discussed in detail here.

3.4 Effect of radiant exitance on 1,4-dioxane degradation

The effects of radiant exitance on 1,4-dioxane degradation were also examined by using our validated model and a virtual annular photoreactor. In the simulation, different radiant exitances (20–100 W/m^2) under laminar (*Re,* 800) or turbulent flow (*Re,* 4000) were examined with SW used as the water (Fig. 6). As the radiant exitance increased, the degradation ratio increased under both flow regimes, which was consistent with our observations in the validation experiments. In contrast, as the radiant exitance increased, the radiation efficiency decreased under both flow regimes. Increasing the radiant exitance proportionally increases the VUV fluence rate at every position in the photoreactor regardless of flow type (Eq. S11). Therefore, the VUV doses of the particles were increased by the same ratio as the radiant exitance was increased, resulting in a decrease of radiation efficiency according to Jensen's inequality (Text S1). VUV dose distribution is important in improving degradation and radiation efficiency.

3.5 Optimization of operating parameters based on EEO analysis

Under the same flow regime in the annular VUV photoreactor, the degradation ratio and the radiation efficiency showed opposite trends as the operating parameters were changed: increasing the flow rate decreased the degradation ratio but increased the radiation efficiency, whereas increasing the radiant exitance increased the degradation ratio but decreased the radiation efficiency. As a consequence, degradation ratio and radiation efficiency could not be improved simultaneously (i.e. the highest removal ratio at the highest efficiency) by adjusting these operating parameters under the same flow regime.

Next, radiation efficiency, which was calculated by using the actual residual ratio and the average VUV dose (Eqs. 11 and 12), was used as an index of cost-effectiveness with respect to radiation energy input. In practical applications, EEO (kWh/(m^3·order)) has been widely used for comparing cost-effectiveness among advanced oxidation processes and operating conditions (Bolton and Stefan, 2002):

$$\mathrm{EEO} = \frac{W_\mathrm{p} + \mathrm{P_l}}{Q \cdot \log_{10}(C_\mathrm{in}/C_\mathrm{out})} \tag{13}$$

where W_p and P_l are the electrical energy input (kW) of the pump and lamp, respectively; Q is the volumetric flow rate (m^3/h); and C_in and C_out are concentrations of 1,4-dioxane at the inlet and outlet of the reactor, respectively. In the present study, because the required pump input (calculated by pressure loss) was much smaller than the lamp power (Text S4), W_p was considered to be negligible in Eq. 13. Based on Eqs. 12 and 13, a connection between radiation efficiency and EEO can be established through the actual log degradation ratio:

$$\mathrm{EEO} = A \cdot \frac{1}{\eta} \cdot \frac{\alpha}{k} \cdot \frac{\mathrm{P_l}}{P_\mathrm{VUV}} \tag{14}$$

where A is the conversion factor to convert watts to kilowatts, the natural logarithm to the common logarithm, and seconds to hours. Assuming the fourth term in Eq. 14 is a constant, EEO is a monotonic function of radiation efficiency. Thus, the results of radiation efficiency in 3.3 and 3.4 can be used to examine EEO with changes in operating parameters. In the present study, we assumed that the average power conversion efficiency of the VUV lamp with the transmittance sleeve (the reciprocal of the fourth term in Eq. 14) was 4.5% (Text S5). As a consequence, the EEO value will decrease as the flow rate increase (under the same flow regime) or the radiation exitance decrease.

Figure 7 shows EEO values calculated by using the radiation efficiencies obtained in the simulations under different flow rates (*Re* 400–4000) and radiant exitances (20–100 W/m^2) for GW in the virtual photoreactor. Under laminar flow (Fig. 7A), EEO was highly sensitive to both flow rate and radiant exitance. EEO decreased with both increasing flow rate, which is in agreement with previous research (Bagheri and Mohseni, 2015), and decreasing radiant exitance, suggesting that VUV treatment using low-power lamps and a high flow rate would be the most economical set-up under laminar flow conditions.

Under turbulent flow (Fig. 7B), EEO was less sensitive to flow rate and radiant exitance compared with under laminar flow. Although the change was limited, EEO decreased with increasing flow rate, which is in agreement with previous research (Bagheri and Mohseni, 2017). Likewise, EEO slightly decreased with decreasing radiant exitance. Overall, at the high flow rate, EEO was insensitive to the changes in radiant exitance. Thus, VUV treatment using high-power lamps and at the high flow rate is recommended under turbulent flow, because the degradation ratio markedly increased with increasing radiant exitance (Fig. S6), even if there was no marked change in EEO.

4. Conclusions

1. A CFD model that takes into account the effects of flow rate and radiant exitance on 1,4-dioxane degradation during VUV treatment was developed. The model required only one parameter, the pseudo-first-order rate constant for the reaction of 1,4-dioxane, which was determined by a simple batch degradation experiment. The model successfully predicted 1,4-dioxane degradation in a pilot-scale flow-through annular photoreactor operated at different flow rates and radiant exitances, confirming the reliability of the model.
2. Model simulation in a virtual photoreactor revealed that both increasing flow rate and decreasing radiant exitance increased radiation efficiency, which was findings that agreed with those from the experiments using the pilot-scale photoreactor.
3. EEO analysis suggested that VUV treatment using low-power lamps and a high flow rate was the most economical set-up under laminar flow. In contrast, treatment using high-power lamps at the high flow rate was suggested to be the most economical set-up under turbulent flow.

Acknowledgments

This research was supported by the Japan Society for the Promotion of Science [grant number 16H06362] and the JST-Mirai Program of the Japan Science and Technology Agency [grant number JPMJMI18DB].

References

Adams, C.D., Scanlan, P.A., Secrist, N.D., 1994. Oxidation and Biodegradability Enhancement of 1,4-Dioxane Using Hydrogen Peroxide and Ozone. Environmental Science and Technology 28, 1812–1818.

Bagheri, M., Mohseni, M., 2017. Pilot-scale treatment of 1,4-dioxane contaminated waters using 185 nm radiation: Experimental and CFD modeling. Journal of Water Process Engineering 19,

185–192.
Bagheri, M., Mohseni, M., 2015. A study of enhanced performance of VUV/UV process for the degradation of micropollutants from contaminated water. Journal of Hazardous Materials 294, 1–8.
Bagheri, M., Mohseni, M., 2014. Computational fluid dynamics (CFD) modeling of VUV/UV photoreactors for water treatment. Chemical Engineering Journal 256, 51–60.
Bolton, J.R., Stefan, M.I., 2002. Fundamental photochemical approach to the concepts of fluence (UV dose) and electrical energy efficiency in photochemical degradation reactions. Research on Chemical Intermediates 28, 857–870.
Coleman, H.M., Vimonses, V., Leslie, G., Amal, R., 2007. Degradation of 1,4-dioxane in water using TiO_2 based photocatalytic and H_2O_2/UV processes. Journal of Hazardous Materials 146, 496–501.
Darbyshire, A.G., Mullin, T., 2005. Transition to turbulence in pipe flow. Fluid Mechanics and its Applications 77, 221–231.
De Laat, J., Gallard, H., Ancelin, S., Legube, B., 1999. Comparative study of the oxidation of atrazine and acetone by H_2O_2/UV, Fe(III)/UV, Fe(III)/H_2O_2/UV and Fe(II) or Fe(III)/H_2O_2. Chemosphere 39, 2693–2706.
Dietz, A.C., Schnoor, J.L., 2001. Advances in Phytoremediation. Environmental Health Perspectives 109, 163–168.
European Communities, 2004. European Union Risk Assessment Report, Alkanes, C.
Furatian, L., Mohseni, M., 2018. Influence of chloride on the 185 nm advanced oxidation process. Chemosphere 199, 263–268.
Hill, R.R., Jeffs, G.E., Roberts, D.R., 1997. Photocatalytic degradation of 1,4-dioxane in aqueous solution. Journal of Photochemistry and Photobiology A: Chemistry 108, 55–58.
Imoberdorf, G., Mohseni, M., 2012. Kinetic study and modeling of the vacuum-UV photoinduced degradation of 2,4-D. Chemical Engineering Journal 187, 114–122.
Li, W., Jain, T., Ishida, K., Liu, H., 2017. A mechanistic understanding of the degradation of trace organic contaminants by UV/hydrogen peroxide, UV/persulfate and UV/free chlorine for water reuse. Environmental Science: Water Research and Technology 3, 128–138.
Matsushita, T., Hirai, S., Ishikawa, T., Matsui, Y., Shirasaki, N., 2015. Decomposition of 1,4-dioxane by vacuum ultraviolet irradiation: Study of economic feasibility and by-product formation. Process Safety and Environmental Protection 94, 528–541.
Matsushita, T., Sugita, W., Ishikawa, T., Shi, G., Nishizawa, S., Matsui, Y., Shirasaki, N., 2019. Prediction of 1,4-dioxane decomposition during VUV treatment by model simulation taking into account effects of coexisting inorganic ions. Water Research 164.
McGuire, M.J., Suffet, I.H., Radziul, J. V, 1978. Assessment of Unit Processes for the Removal of Trace Organic Compounds From Drinking Water. Journal - American Water Works Association 70, 565–572.
Mohr, T.K.G., DiGuiseppi, W.H., Hatton, J.W., Anderson, J.K., 2020. Environmental investigation and remediation: 1, 4-dioxane and other solvent stabilizers. CRC Press.
Oppenlander, T., 2007. Mercury-free sources of VUV/UV radiation: application of modern excimer lamps (excilamps) for water and air treatment. journal of 6, 253–264.
Patton, S., Li, W., Couch, K.D., Mezyk, S.P., Ishida, K.P., Liu, H., 2017. Impact of the ultraviolet photolysis of monochloramine on 1,4-dioxane removal: New insights into potable water reuse. Environmental Science and Technology Letters 4, 26–30.
Sharpless, C.M., Linden, K.G., 2003. Experimental and model comparisons of low- and medium-pressure Hg lamps for the direct and H2O2 assisted UV photodegradation of N-nitrosodimethylamine in simulated drinking water. Environmental Science and Technology 37, 1933–1940.
Stepien, D.K., Diehl, P., Helm, J., Thoms, A., Püttmann, W., 2014. Fate of 1, 4-dioxane in the aquatic environment: From sewage to drinking water. Water Research 48, 406–419.
Suh, J.H., Mohseni, M., 2004. A study on the relationship between biodegradability enhancement

and oxidation of 1,4-dioxane using ozone and hydrogen peroxide. Water Research 38, 2596–2604.
USEPA, 2013. Summary on 1,4-Dioxane (123-91-1) 1–16.
Versteeg, H.K., Malalasekera, W., 2007. An introduction to computational fluid dynamics: the finite volume method.
Weimar, R., 1980. Prevent groundwater contamination before it's too late. Water & Waste Engineering 17, 30–33.
WHO, 2005. 1,4-Dioxane in Drinking-water.Background document for preparation of WHO Guidelines for drinking-water quality.
Wols, B.A., Harmsen, D.J.H., van Remmen, T., Beerendonk, E.F., Hofman-Caris, C.H.M., 2015. Design aspects of UV/H2O2 reactors. Chemical Engineering Science 137, 712–721.
Wols, B.A., Hofman-Caris, C.H.M., 2012a. Modelling micropollutant degradation in UV/H 2O 2 systems: Lagrangian versus Eulerian method. Chemical Engineering Journal 210, 289–297.
Wols, B.A., Hofman-Caris, C.H.M., 2012b. Review of photochemical reaction constants of organic micropollutants required for UV advanced oxidation processes in water. Water Research 46, 2815–2827.
Wols, B.A., Hofman, J.A.M.H., Beerendonk, E.F., Uijttewaal, W.S.J., van Dijk, J.C., 2011. A systematic approach for the design of UV reactors using computational fluid dynamics. AIChE Journal 57, 193–207.
Xie, P., Yue, S., Ding, J., Wan, Y., Li, X., Ma, J., Wang, Z., 2018. Degradation of organic pollutants by Vacuum-Ultraviolet (VUV): Kinetic model and efficiency. Water Research 133, 69–78.
Zenker, M.J., Borden, R.C., Barlaz, M.A., 2003. Occurrence and Treatment of 1,4-Dioxane in Aqueous Environments. Environmental Engineering Science 20, 423–432.

Table 1. Lamps and quartz sleeves used in the present study.

Low-pressure mercury lamp	Quartz sleeve	Exitance on the external surface of the quartz sleeve (W/m^2)	
		185 nm	254 nm
240 W	Low transmittance	60.1 ± 1.3	497 ± 31
65 W		25.6 ± 1.8	229 ± 8
65 W with coating		7.3 ± 0.9	161 ± 14
240 W	High transmittance	105 ± 4.0	548 ± 27
65W		40.3 ± 2.2	247 ± 9
65 W with coating		13.9 ± 1.2	173 ± 16

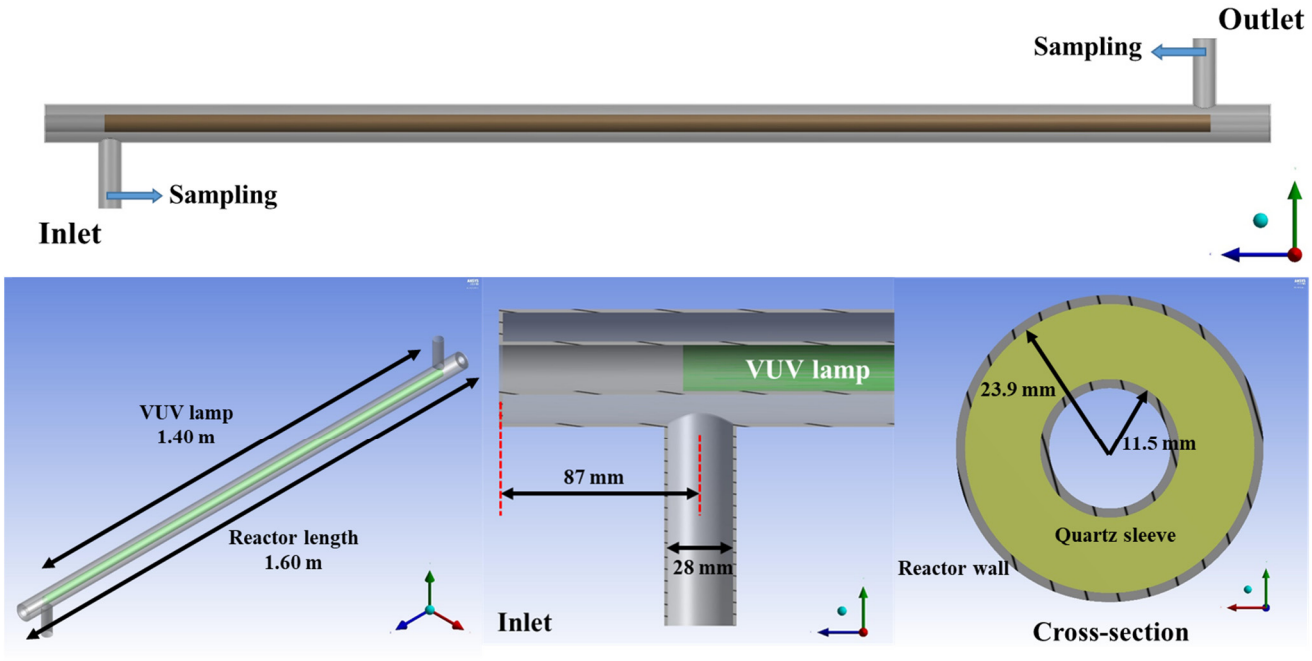

Figure 1. Schematic of the pilot-scale flow-through annular photoreactor. VUV, vacuum ultraviolet.

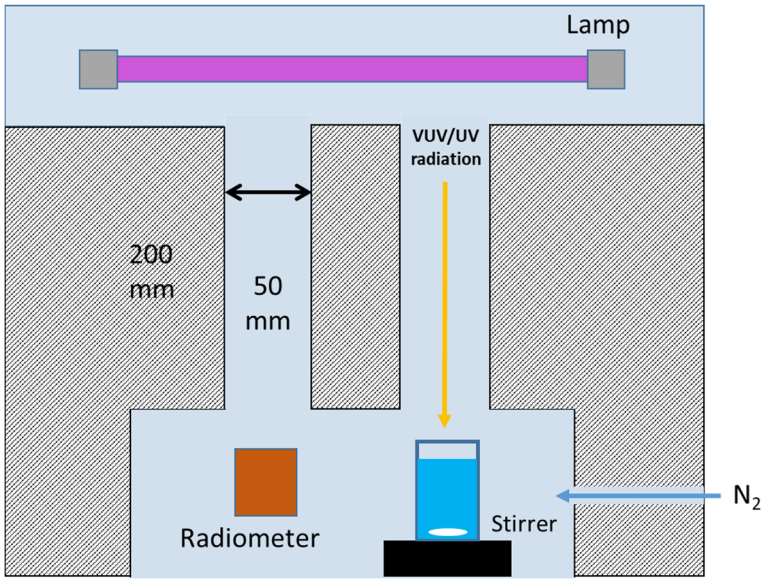

Figure 2. Schematic of the quasi-collimated beam VUV apparatus. VUV, vacuum ultraviolet.

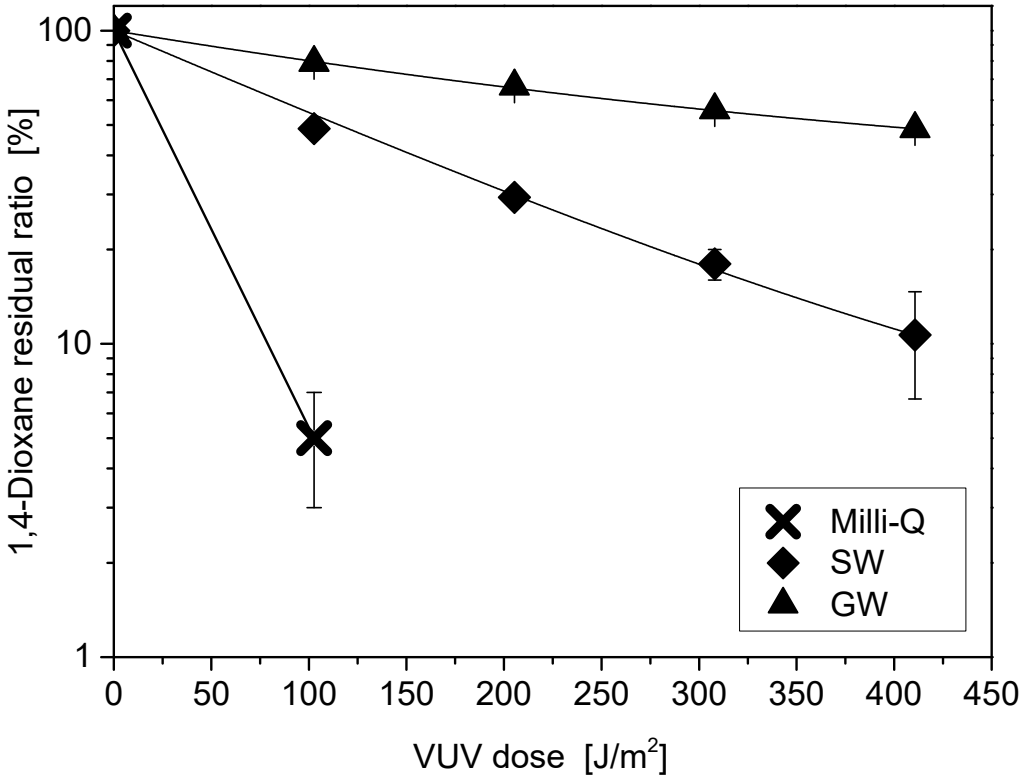

Figure 3. Degradation of 1,4-dioxane in Milli-Q water, synthetic water (SW), and groundwater (GW) in batch experiments using a quasi-collimated beam radiation reactor. Error bars indicate standard deviations of three experiments. VUV, vacuum ultraviolet.

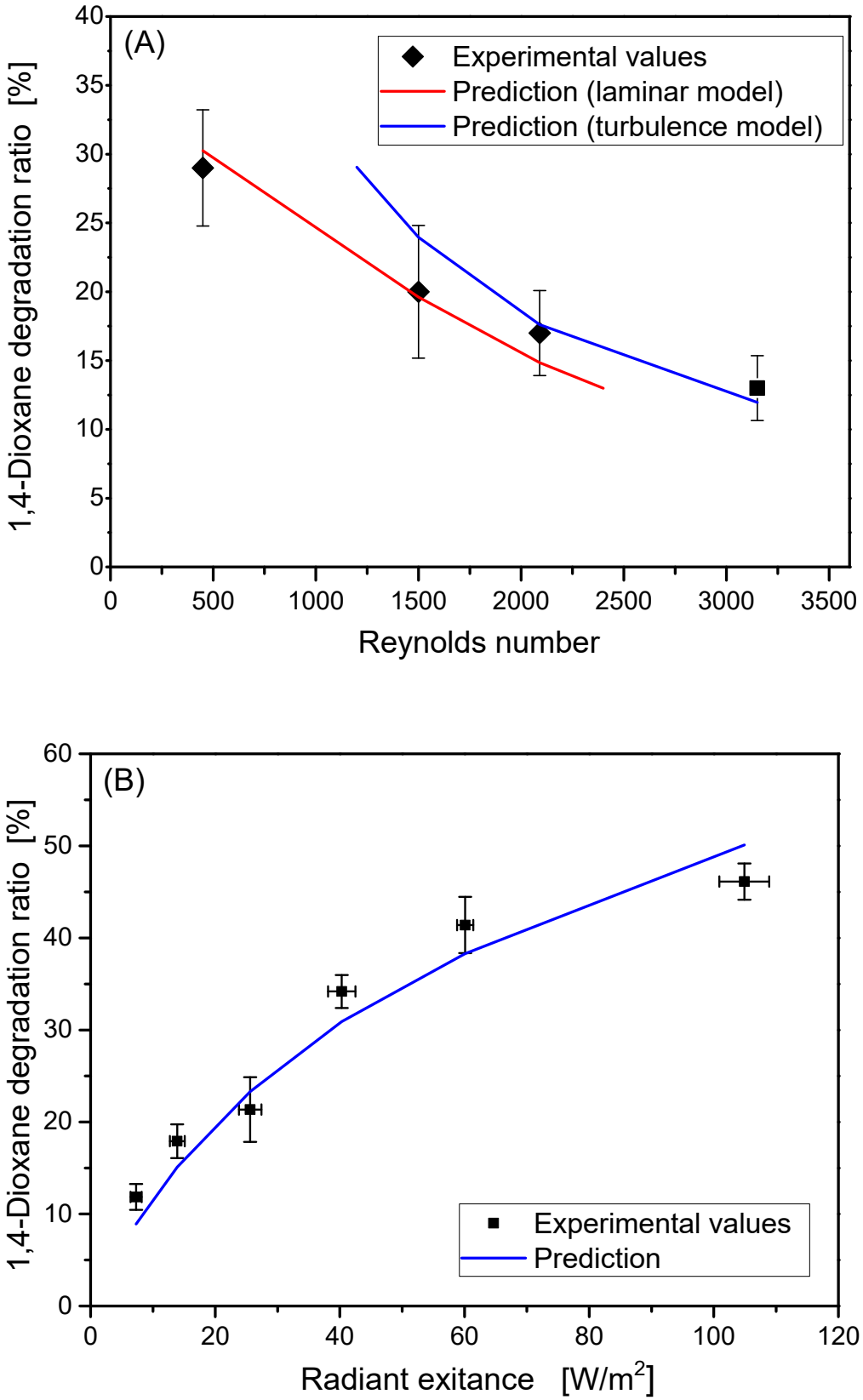

Figure 4. Comparison of predicted and experimental 1,4-dioxane degradation ratios in a pilot-scale flow-through annular photoreactor (A) at different flow rates and a radiant exitance of 105 W/m^2 using sampled groundwater and (B) at a flow rate of 6.96 L/m (Reynolds number, 2100) at different radiant exitances using synthetic water. Error bars indicate standard deviations of at least three experiments.

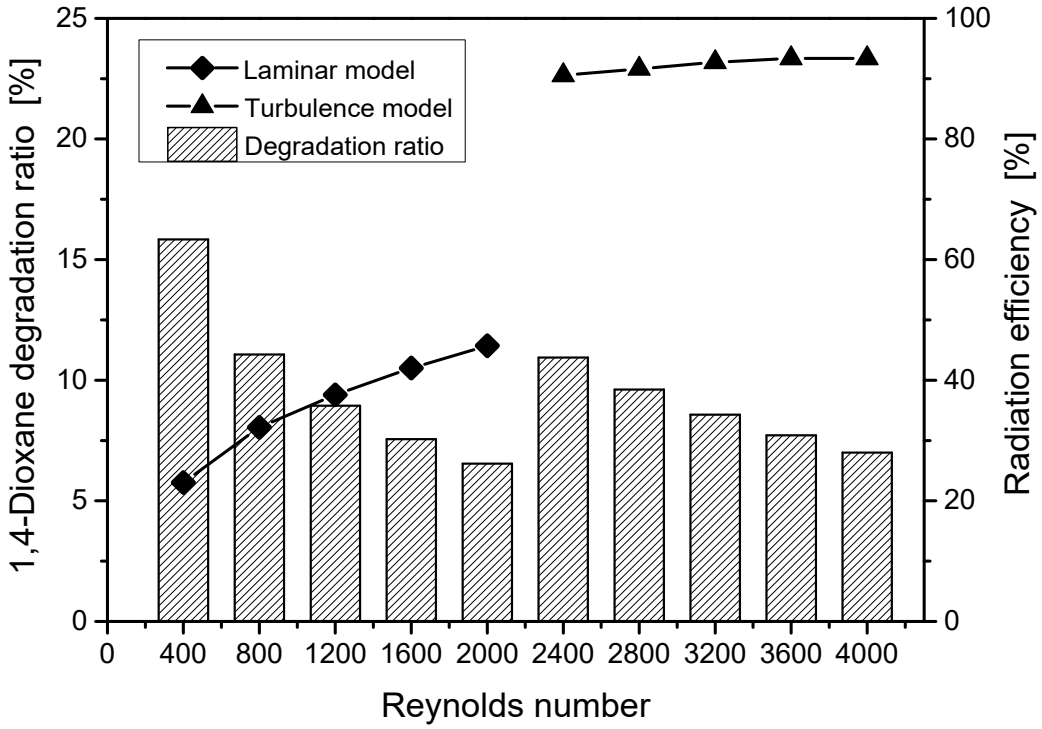

Figure 5. Effect of flow rate (i.e., Reynolds number) on 1,4-dioxane degradation ratio and radiation efficiency in an ideal photoreactor.

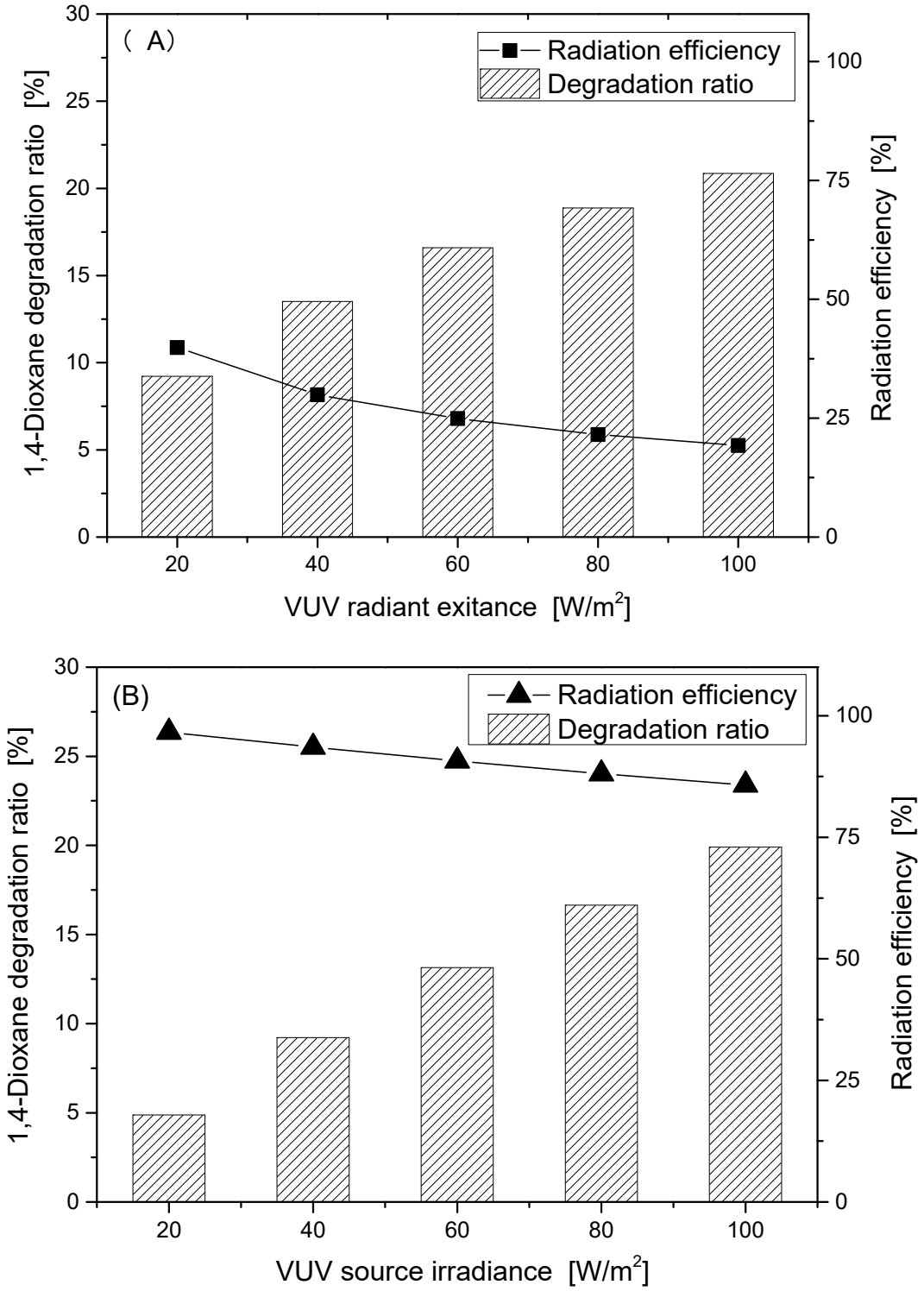

Figure 6. Effect of radiation exitance on 1,4-dioxane degradation ratio and radiation efficiency in a simulated annular photoreactor operated under laminar flow (*Re*, 800) (A) or turbulent flow (*Re*, 4000) (B). VUV, vacuum ultraviolet.

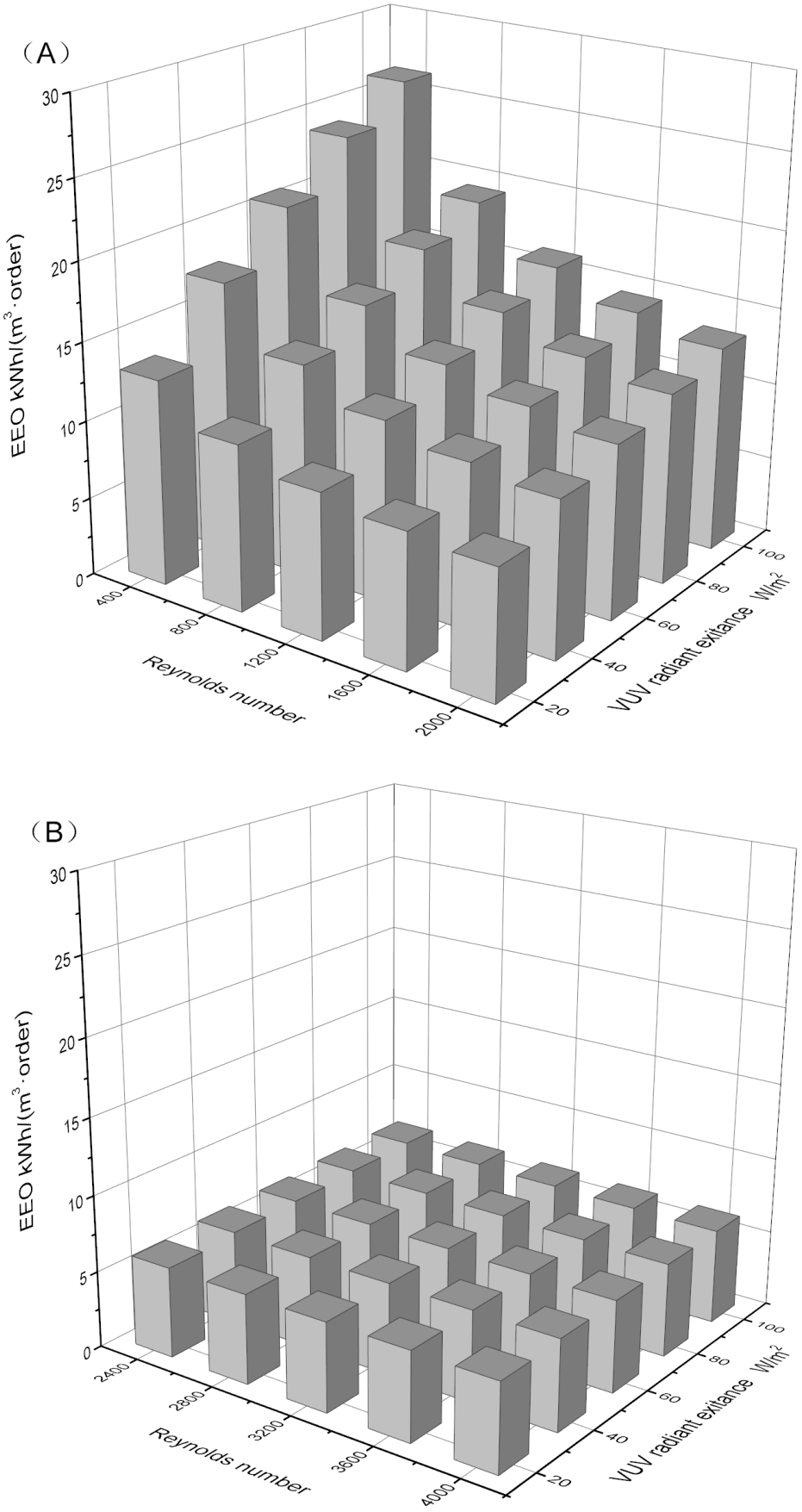

Figure 7. Effects of flow rate (i.e., Reynolds number) and radiant exitance on electrical energy per order (EEO) in an ideal annular photoreactor operated under laminar flow (A) or turbulent flow (B). VUV, vacuum ultraviolet.

Supplementary materials for:

Computational fluid dynamics–based modeling and optimization of flow rate and radiant exitance for 1,4-dioxane degradation in a vacuum ultraviolet photoreactor

Gang Shi[a], Shota Nishizawa[a], Taku Matsushita[b,*], Yuna Kato[a], Takahiro Kozumi[a], Yoshihiko Matsui[b], Nobutaka Shirasaki[b]

[a]Graduate School of Engineering, Hokkaido University, N13W8, Sapporo, 060-8628, Japan

[b]Faculty of Engineering, Hokkaido University, N13W8, Sapporo, 060-8628, Japan

Text S1 Convex function, Jensen's inequality

In mathematics, a real-valued function is said to be convex if the line segment between any two points on the graph of the function lies above or on the graph. For a real convex function (φ), if numbers $x_1, x_2, \cdots, x_n$ are in its domain and of positive weight (w_i), Jensen's inequality can be stated as:

$$\varphi\left(\frac{\sum w_i x_i}{\sum w_i}\right) \leq \frac{\sum w_i \cdot \varphi(x_i)}{\sum w_i} \tag{S1}$$

in which equality holds if and only if $x_1 = x_2 = \cdots = x_n$.

In the present study, Eq. 8

$$C_i = C_0 \cdot \exp(-k \cdot D_i)$$

where C_i is a convex function of D_i, and w_i ($\sum w_i = 1$) is the mass-flux weight, then the mass-flux weight averaged concentration calculated by Eq. 9 has a minimum value:

$$\bar{C} = \sum(w_i C_0 \exp(-kD_i)) \geq C_0 \exp(-k \cdot \sum w_i D_i) = C_{\min} \tag{S2}$$

Equality holds if and only if $D_1 = D_2 = \cdots = D_n$, in other words, no variation in VUV dose among the particles.

Giving the same decrement ratio (m, from 0 to 1) in vacuum ultraviolet (VUV) dose to all of the particles, then

$$D_i' = (1 - m) \cdot D_i \tag{S3}$$

$$\bar{D}' = (1 - m) \cdot \bar{D} \tag{S4}$$

$$\ln\left(\frac{C'_{\min}}{C_0}\right) = -k \cdot \sum w_i D_i' = -k \cdot \bar{D}' = -\mathrm{k} \cdot (1 - m) \cdot \bar{D} > -\mathrm{k} \cdot \bar{D} \tag{S5}$$

$$\ln\left(\frac{\bar{C}'}{C_0}\right) = \ln\left(\sum\left(w_i \cdot \exp\left(-kD_i'\right)\right)\right) = \ln\left(\sum\left(w_i \cdot \exp(-k(1-m)\cdot D_i)\right)\right)$$

$$> \ln(\sum(w_i \cdot \exp(-k \cdot D_i))) \tag{S6}$$

$$\eta' = \frac{\ln\left(\frac{\bar{C}'}{C_0}\right)}{\ln\left(\frac{C'_{\min}}{C_0}\right)} = -\frac{\ln(\sum(w_i \cdot \exp(-k(1-m)\cdot D_i)))}{\mathrm{k}\cdot(1-m)\cdot\bar{D}} \tag{S7}$$

Since $0 < \eta, \eta' < 1$, $\ln\left(\frac{\bar{C}'}{C_0}\right) < 0$

$$\eta' = -\frac{\ln(\sum(w_i \cdot \exp(-k(1-m)\cdot D_i)))}{\mathrm{k}\cdot(1-m)\cdot\bar{D}} > -\frac{\ln(\sum(w_i \cdot \exp(-k(1-m)\cdot D_i)))}{\mathrm{k}\cdot\bar{D}}$$

$$> -\frac{\ln(\sum(w_i \cdot \exp(-k\cdot D_i)))}{\mathrm{k}\cdot\bar{D}} = \eta \tag{S8}$$

As a result, reducing the VUV dose to all of the particles by the same ratio leads to an increase in radiation efficiency.

Text S2 Mass-flow averaged VUV dose ($\bar{D}$)

An annular photoreactor is considered an axisymmetric system where the water is flowing parallel to the lamp, which allows us to simplify the system from three dimensions to two dimensions (*r*-*z*). In the very limited interval of the *z*-direction (d*z*), the instantaneous velocity (*u(r)*) in the *z*-direction and the fluence rate (*I(r)*) are considered to be constant, which means that the VUV dose (*dD*) in this limited interval of the *z*-direction can be calculated as

$$\mathrm{d}D(r) = I(r) \cdot \frac{\mathrm{d}z}{u(r)} \tag{S9}$$

The mass-flow averaged VUV dose in this limited interval is

$$\Delta\bar{D} = \frac{\int_0^{2\pi}\int_{r_q}^{R} \mathrm{d}D(r)\cdot u(r)\mathrm{d}r\mathrm{d}\theta}{\int_0^{2\pi}\int_{r_\mathrm{q}}^{R} u(r)\mathrm{d}r\mathrm{d}\theta} = \frac{\int_0^{2\pi}\int_{r_\mathrm{q}}^{R} \mathrm{d}D(r)\cdot u(r)\mathrm{d}r\mathrm{d}\theta}{Q} \tag{S10}$$

where r_q is the external radius of the quart sleeve, R is the internal radius of the photoreactor, and Q is the flow rate. *I(r)* can be calculated by the Beer–Lambert law:

$$I(r) = I_0 \cdot \frac{r_\mathrm{q}}{r} \cdot 10^{-\alpha(r-r_\mathrm{q})} \tag{S11}$$

where I_0 is the radiant exitance on the external surface of the quartz sleeve, and α is the absorption coefficient of water calculated by

$$\alpha = \frac{\log_{10}(T_{10,w})}{0.01\ m} \tag{S12}$$

where $T_{w,10}$ is the 10-mm transmittance of water. If L is the length of the VUV lamp, then the mass-flow average VUV dose for the water flow through the photoreactor is

$$\overline{D} = \int_0^L \frac{\int_0^{2\pi}\int_{r_q}^{R} dD(r)\cdot u(r) dr d\theta}{Q} = \frac{2\pi r_q L I_0}{Q\alpha}\left(1 - 10^{-\alpha(R-r_q)}\right) \quad \text{(S13)}$$

If $h = R - r_q$ is the thickness of the water layer, $1 - 10^{-\alpha(R-r_q)}$ is very close to 1, and $2\pi r_q L I_0$ is the total VUV radiation input from the surface of the quartz sleeve to the system (P_{VUV}), then the mass-flow averaged VUV dose becomes

$$\overline{D} = \frac{P_{VUV}}{Q\alpha}\cdot\left(1 - 10^{-\alpha h}\right) \approx \frac{P_{VUV}}{Q\alpha} \quad \text{(S14)}$$

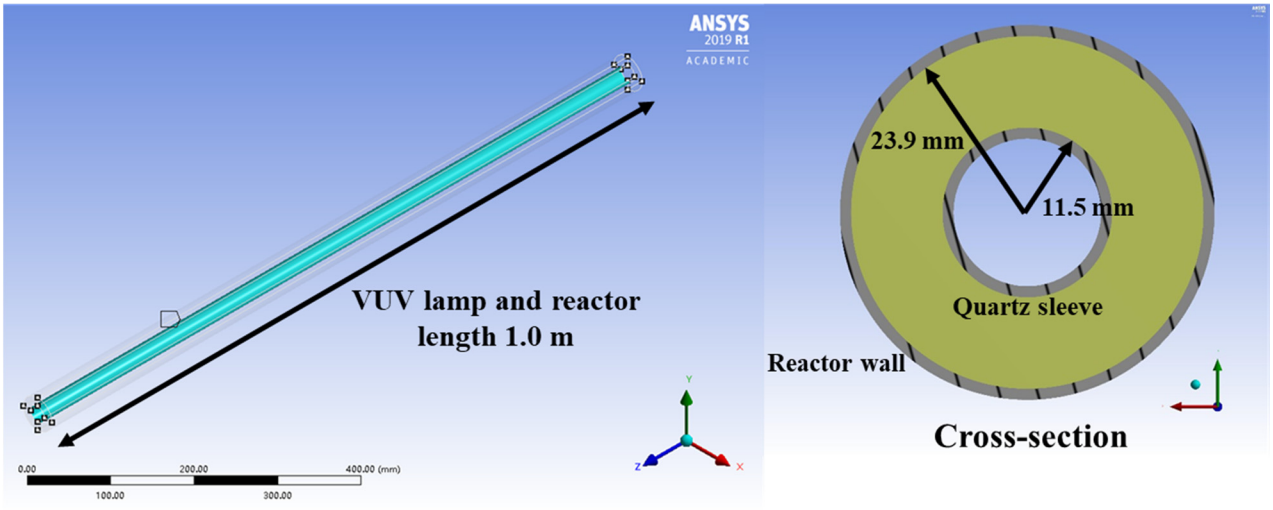

Figure S1. Schematic of the ideal annular photoreactor. VUV, vacuum ultraviolet.

Table S1. Chemical properties of the natural groundwater (Tachikawa, Japan) and synthetic water used in the present study

Property	Groundwater	Synthetic water
pH	7.8	7.8
*DOC (mg/L)	0.09	0.12
1,4-Dioxane (μg/L)	36	100
Alkalinity (mg/L $CaCO_3$)	44	44
Na^+	666	768
K^+	35	44
NH_4^+	0	0
Mg^{2+}	505	73
Ca^{2+} (μmol/L)	1146	293
Cl^-	605	482
NO_3^-	452	17
NO_2^-	0	0
SO_4^{2-}	354	139
*VUV absorption coefficient (cm^{-1})	2.84	2.77

*DOC - dissolved organic carbon.

*VUV - vacuum ultraviolet. At 185 nm, the absorption coefficient of water is 1.8 cm^{-1} (common logarithm), and the molar extinction coefficients of the inorganic ions are as follows (Imoberdorf and Mohseni, 2011; Weeks et al., 1963):

	SO_4^{2-}	Cl^-	HCO_3^-	CO_3^{2-}
$L \cdot mol^{-1} \cdot cm^{-1}$	186	3.6×10^{-3}	1.1×10^3	1.75×10^3

$$2[CO_3^{2-}] + [HCO_3^-] + [OH^-] = 2 \times \frac{\text{Alkalinity}\left(\frac{mg}{L}CaCO3\right)}{100\frac{g}{mol}} \times 10^{-3}\ g/mg \quad (S15)$$

$$HCO_3^- \rightleftharpoons CO_3^{2-} + H^+ \qquad Ka_2 = \frac{[CO_3^{2-}][H^+]}{[HCO_3^-]} = 4.2 \times 10^{-11} \quad (S16)$$

The concentrations of carbonate and bicarbonate were 2.6×10^{-6} and 8.8×10^{-4}, respectively.

Using these values, the absorption coefficient of the groundwater can be calculated with the concentrations shown in Table S1:

$$a_{GW} = 1.8 + (186 \times 354 \times 10^{-6}) + (3.6 \times 10^{-3} \times 605 \times 10^{-6}) + (1.1 \times 10^3 \times 8.8 \times 10^{-4}) + (1.75 \times 10^3 \times 2.6 \times 10^{-6}) = 2.84\ cm^{-1} \quad (S17)$$

Similarly, the absorption coefficient of SW was calculated as:

$$a_{SW} = 1.8 + (1.1 \times 10^3 \times 8.8 \times 10^{-4}) + (1.75 \times 10^3 \times 2.6 \times 10^{-6}) = 2.77\ cm^{-1} \quad (S18)$$

Text S3 VUV dose of the samples in the batch experiment (exposed to a quasi-collimated beam)
As described by Bolton and Stefan (2002), the volume average VUV fluence rate (E_{avg}) can be corrected by using the radiometer reading (E_0) and four other parameters:

$$E_{\mathrm{avg}} = E_0 \cdot RF \cdot PF \cdot WF \cdot DF \quad \text{(S19)}$$

(1) Reflection Factor (*RF*)
RF accounts for the portion of the VUV incident beam that is reflected at the fluid/gas interface. The fraction of the incident beam (*R*) that is reflected is given by Fresnel's law:

$$R = \frac{(n_1 - n_2)^2}{(n_1 + n_2)^2} \quad \text{(S20)}$$

where n_1 and n_2 are the refractive indices of the two media. Using approximate values of $n_1 = 1.000$ (air) and $n_2 = 1.372$ (water), R = 0.025. Therefore,

$$RF = 1 - R = 0.975 \quad \text{(S21)}$$

(2) Petri Factor (*PF*)
PF accounts for the non-uniformity of the radiation field across the irradiation plane and is defined as the incident irradiance averaged over the top of the vessel containing the solution (a beaker in the present study) divided by the incident irradiance at the center of the plane. In the present study, the PF of the quasi-collimated beam radiation reactor was 0.65.

(3) Water Factor (*WF*)
WF corrects for attenuation of the incident fluence rate due to absorption in the irradiated column:

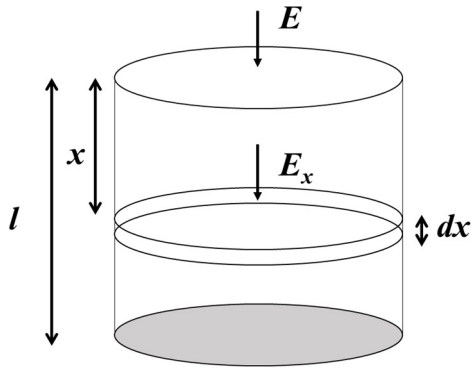

where *l* is the depth of the water, *E* is the incident photon fluence rate at the center of the water surface, E_x is the photon fluence rate at depth *x* determined by the Beer–Lambert law:

$$E_x = E \cdot 10^{-\alpha x} \quad \text{(S22)}$$

where α is the absorption coefficient of the solution at 185 nm (common logarithm), the absorbed irradiation in the infinitesimal slice, which is given by

$$E_{a,x} = E \cdot 10^{-\alpha x}\left(1 - 10^{-\alpha \mathrm{d}x}\right) \quad \text{(S23)}$$

A Taylor series expansion of $10^{-\alpha dx}$ with retention of the terms up to the one linear in dx gives

$$E_{a,x} \approx E \cdot 10^{-\alpha x} \cdot \ln 10 \cdot a\mathrm{d}x \quad \text{(S24)}$$

The overall absorbed irradiation (E_a) in the total solution is given by integrating from 0 to l:

$$E_a = \int_0^l E \cdot 10^{-\alpha x} \cdot \ln 10 \cdot a\mathrm{d}x = E \cdot (1 - 10^{-\alpha l}) \quad \text{(S25)}$$

Because $1 - 10^{-al}$ is very close to 1, the WF equals 1.

(4) Divergence Factor (*DF*)
DF is needed because the beam in the reactor is not fully collimated. DF is given by

$$DF = \frac{L}{L+l} \quad \text{(S26)}$$

where L is the distance from the VUV radiation source to the top of the water sample. In the present study, the *DF* was 0.90. The VUV dose is calculated by multiplying the volume average VUV fluence rate (E_{avg}) by the irradiation time.

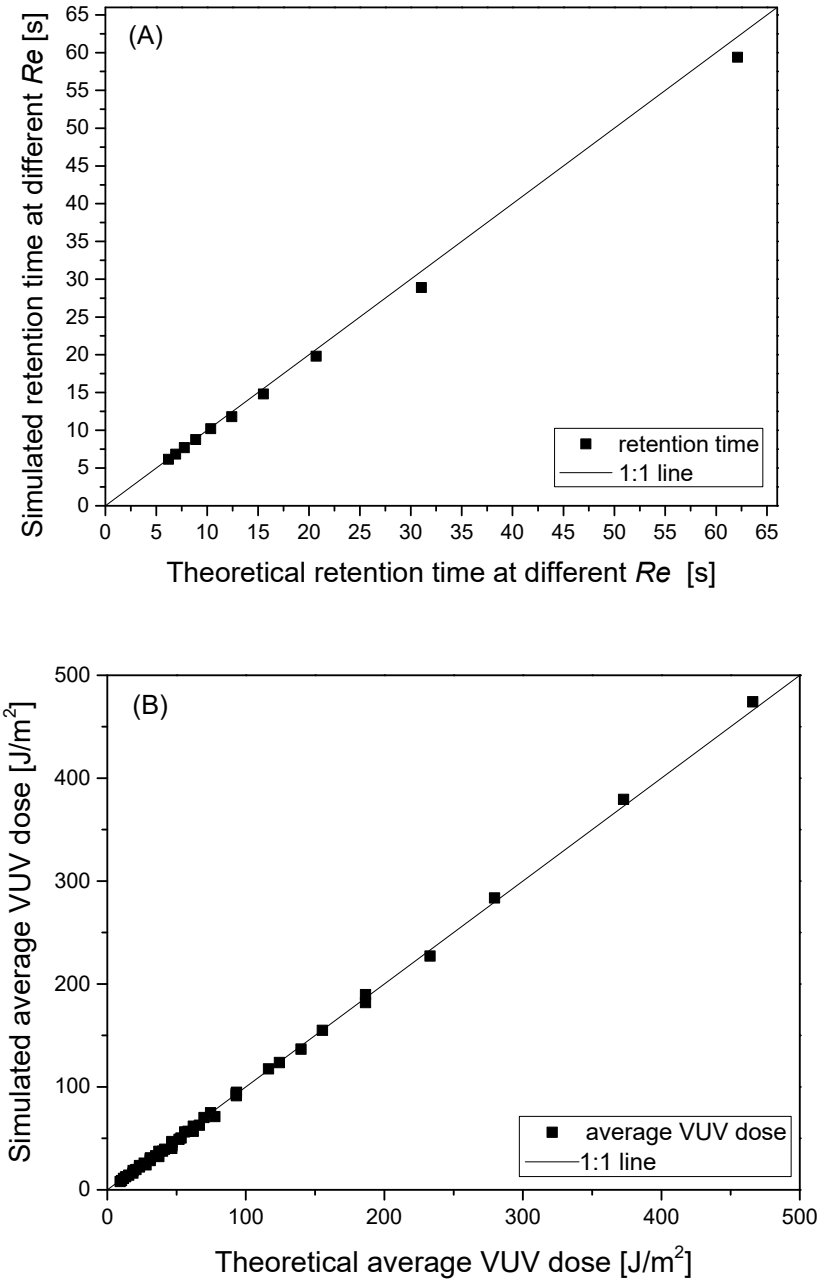

Figure S2. Comparison of simulated and theoretical values of retention time (A) and average vacuum ultraviolet (VUV) dose (B) in an ideal photoreactor. The simulated values were obtained by computational fluid dynamics particle-based simulation. Re, Reynolds number.

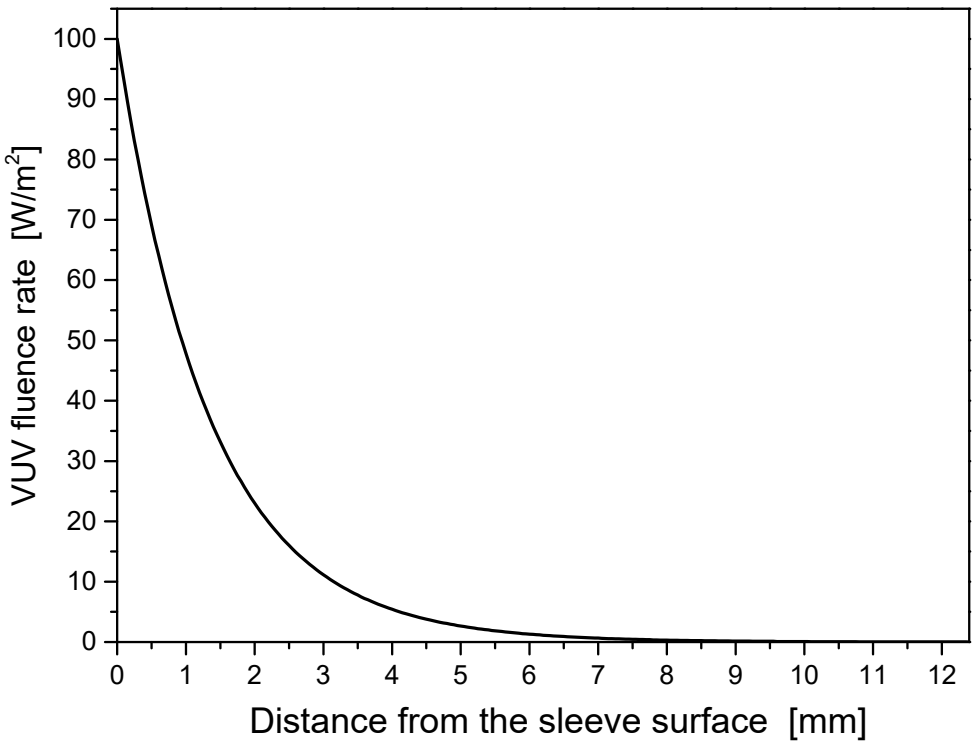

Figure S3. Vacuum ultraviolet (VUV) fluence rate in groundwater across the photoreactor radius.

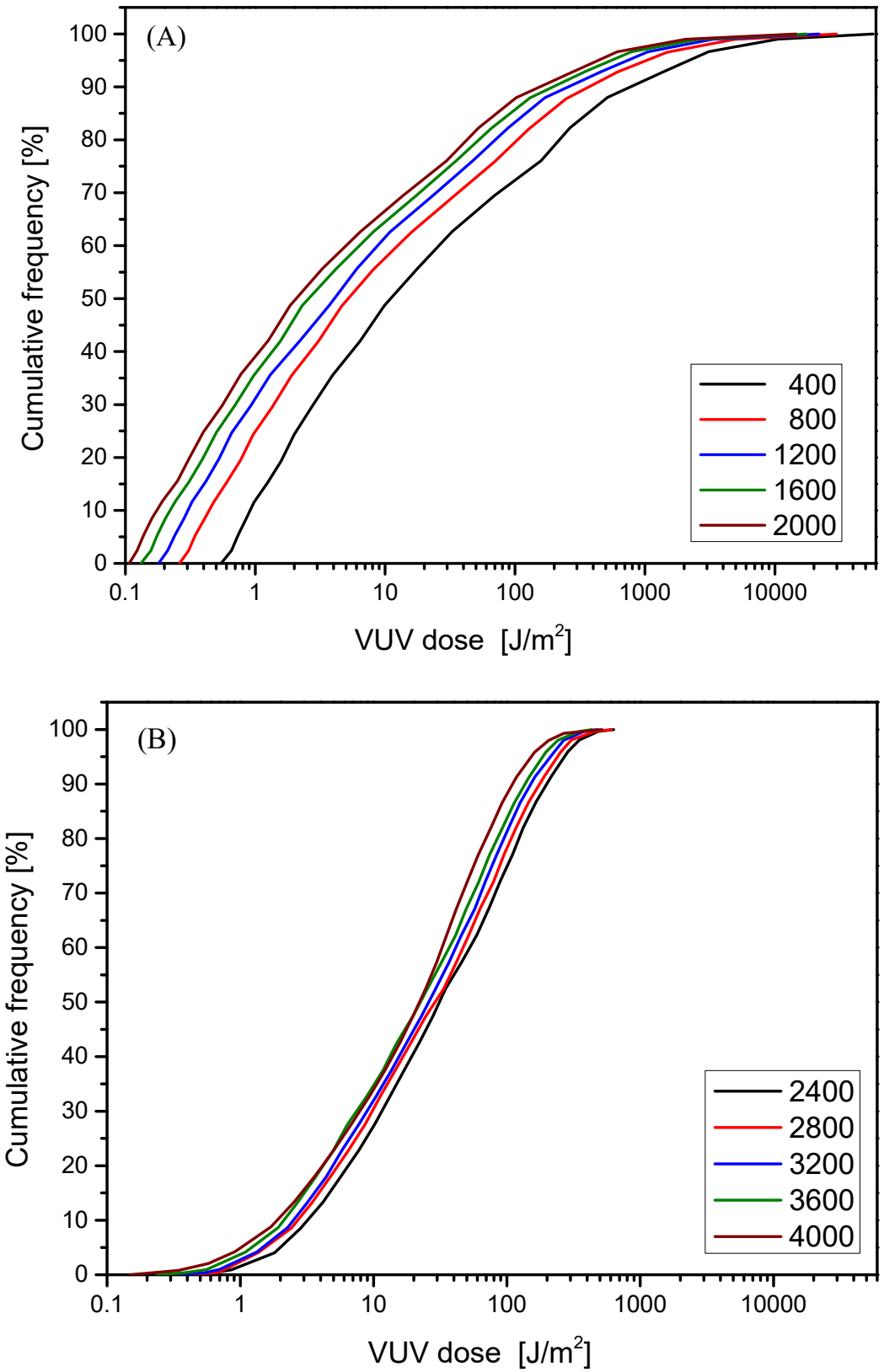

Figure S4. Cumulative vacuum ultraviolet (VUV) dose distribution under laminar flow (A) or turbulent flow (B). The numbers in the legends are Reynolds numbers.

Text S4 Required pump input calculated by pressure loss

In Eq. 13 in the main text, the required pump input can be calculated by using

$$W_{\mathrm{p}}\ [W] = \frac{Q\ [\mathrm{m}^3/\mathrm{s}]\cdot \Delta P[\mathrm{Pa}]}{\epsilon} \tag{S27}$$

where Q is the flow rate, ΔP is the pressure loss, and ϵ is the pump electrical efficiency (normally 50%–75%) (Bagheri and Mohseni, 2015).

In the present study, the maximum pressure loss was 42 Pa at Re 4000, meaning that the maximum required pump input is

$$W_{\mathrm{p}} = \frac{2.2 \times 10^{-4}\frac{\mathrm{m}}{\mathrm{s}} \times 42\ \mathrm{Pa}}{50\%} \approx 0.02\ \mathrm{W} \tag{S28}$$

Compared with the VUV lamp power (>30 W), W_{p} is considered to be negligible.

Text S5 Relationship between power input and total VUV radiation output

In Eq. 14 in the main text, the fourth term is affected by the VUV lamp. To simplify the relationship between radiation efficiency and electrical energy by order, we assumed that the ratio of VUV radiation output on the surface of the quartz sleeve to VUV lamp electricity input is a constant (ε, power conversion efficiency). The calculation method for ε is as follows. In the pilot-scale reactor, the external surface of the sleeve can be expressed as

$$S = 2\pi rL = 0.101\ \mathrm{m}^2 \tag{S29}$$

For the 240-W VUV lamp, the radiation exitance on the sleeve is 105 W/m^2, giving a VUV output of

$$P_{\mathrm{VUV}} = \gamma \cdot S = 105 \times 0.101\ \mathrm{W} = 10.6\ \mathrm{W} \tag{S30}$$

Thus, the power conversion efficiency for the 240-W VUV lamp is

$$\varepsilon = \frac{P_{\mathrm{VUV}}}{P_{\mathrm{input}}} \times 100\% = \frac{10.6}{240} \times 100\% = 4.4\% \tag{S31}$$

For the 65-W VUV lamp, the radiation exitance on the sleeve is 40.3 W/m^2, giving a VUV output of

$$P_{\mathrm{VUV}} = \gamma \cdot S = 40.3 \times 0.101\ \mathrm{W} = 4.07\ \mathrm{W} \tag{S32}$$

Thus, the power conversion efficiency for the 65-W VUV lamp is

$$\varepsilon = \frac{P_{\mathrm{VUV}}}{P_{\mathrm{input}}} \times 100\% = \frac{4.07}{65} \times 100\% = 6.3\% \tag{S33}$$

Plotting P_{input} on the X-axis and P_{VUV} on the Y-axis and then fitting a straight line through the coordinate origin affords $\varepsilon \approx 4.5\%$ (Fig. S5).

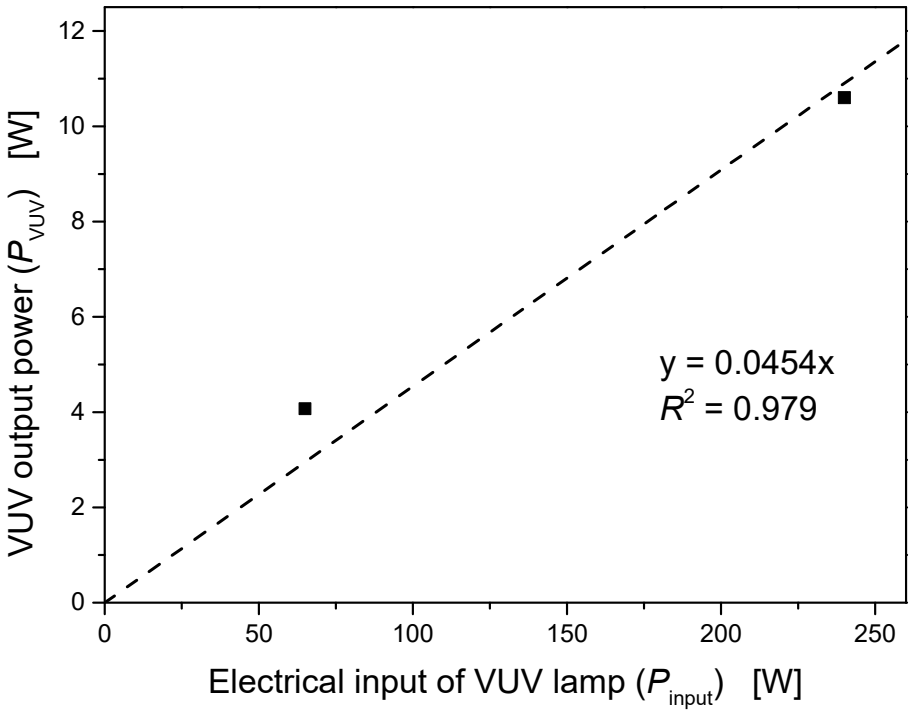

Figure S5. Linear fitting between electrical input and vacuum ultraviolet (VUV) energy output for the VUV lamp.

The VUV radiant exitance (γ) in the simulation and equivalent electrical power input (*P*) were calculated and are shown in Table S2.

Table S2. VUV radiant exitance (γ) in the simulation and equivalent electrical power input (*P*) calculated by using power conversion efficiency of the VUV lamps

γ (W/m^2)	20	40	60	80	100
P (W)	31	63	94	126	157

*γ - radiant exitance on the external surface of the sleeve.

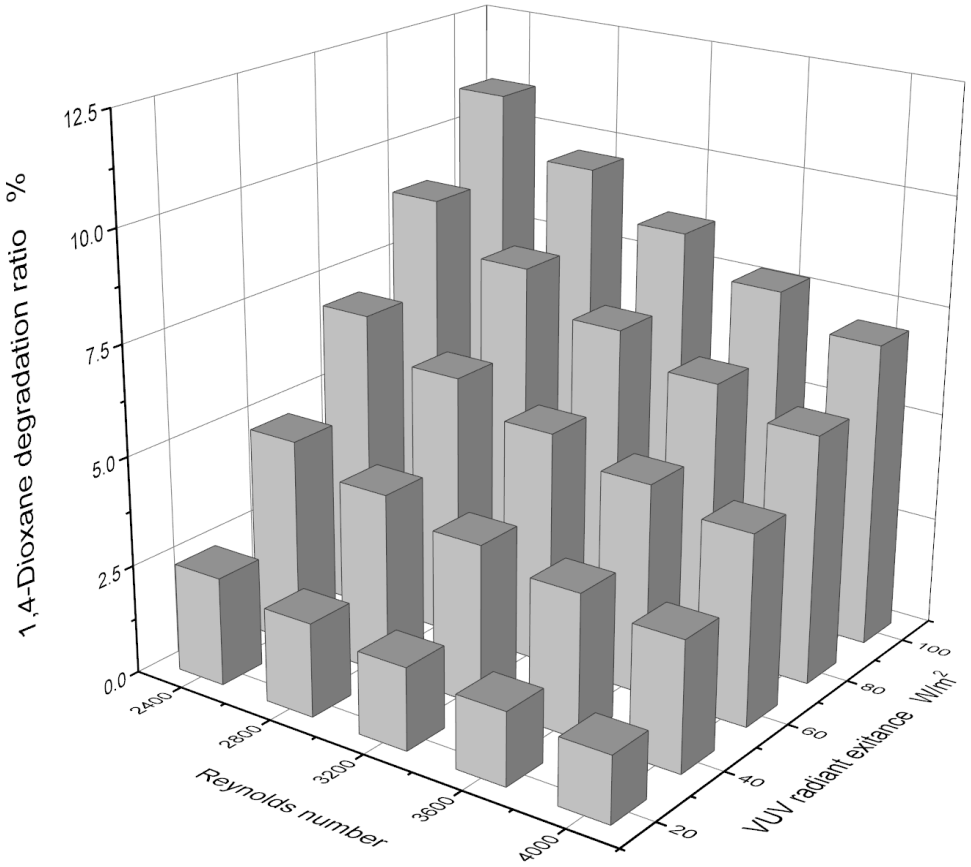

Figure S6. Degradation ratio of 1,4-dioxane under turbulent flow in an ideal photoreactor, as determined by computational fluid dynamics simulation. VUV, vacuum ultraviolet.

References

Bagheri, M., Mohseni, M., 2015. A study of enhanced performance of VUV/UV process for the degradation of micropollutants from contaminated water. J. Hazard. Mater. 294, 1–8.

Bolton, J.R., Stefan, M.I., 2002. Fundamental photochemical approach to the concepts of fluence (UV dose) and electrical energy efficiency in photochemical degradation reactions. Res. Chem. Intermed. 28, 857–870.

Imoberdorf, G., Mohseni, M., 2011. Degradation of natural organic matter in surface water using vacuum-UV irradiation. J. Hazard. Mater. 186, 240–246.

Weeks, J.L., Meaburn, G.M.A., Gordon, S., 1963. Absorption coefficients of liquid water and aqueous solutions in far ultraviolet. Radiat. Res. 19, 559-.